

A generalized scheme for characterizing orientational correlations in condensed phases of high symmetry molecules. Demonstration for SF₆ and C₆₀

László Temleitner^{1, a)}

Institute for Solid State Physics and Optics, Wigner Research Centre for Physics, H-1121 Budapest, Konkoly Thege út 29-33., Hungary

(Dated: 14 January 2021)

The orientational correlation scheme introduced earlier for tetrahedral molecules is extended for being able to classify orientational correlations between pairs of high symmetry molecules. It is based on the number of corner atoms of each molecule found within the orientation cones and provides the probability of 6 orientation groups versus the centre-centre distance. The apex of the orientation cone coincides with the molecular centre and the axis points towards the other centre, while the apex angle is chosen, that the average coordination number of the corner atoms inside would be 2. The method is applicable to molecules whose corner atoms are spaced evenly and only 1, 2, or 3 corner atoms must be found inside the cone. To demonstrate the applicability of the method, the plastic crystalline phase of the truncated icosahedral shaped C₆₀ molecules and the octahedral-shaped SF₆ molecules in its gaseous, supercritical fluid, liquid and plastic crystalline phases have been modeled using classical molecular dynamics. For SF₆, after the best performing forcefield, in terms of the density and the total scattering structure factor, was found, orientational correlations have been analyzed. In the non-crystalline phases, close contact orientation and medium-range order regions could be identified. While the former is invariant to the changes of the density, the latter showed longer-ranged correlations as density raised. In the plastic crystalline state, fluorine atoms are oriented along the lattice directions with higher probability. In C₆₀, local order in the first and second coordination shells is determined quantitatively for three force fields.

I. INTRODUCTION

A most important issue in the structure analysis of disordered materials is to find suitable and simple representation(s) of the studied material that can emphasize its characteristic property. Considering orientational correlations in condensed phases of high-symmetry molecules (including whose shape belonging to the most symmetrical ones called 'Platonic solids': tetrahedron, octahedron, cube, icosahedron and dodecahedron), there is a lack of suitable descriptions: atomic radial distribution function (RDF, $g(r)$) analysis is a frequently applied method, but it does not take into account the symmetry of molecules in a direct way. On the other hand, the application of symmetry adapted functions is restricted mainly to crystalline phases. In 2007 Rey¹ introduced a scheme that classify any mutual arrangement between pairs of tetrahedral molecules to an ideal arrangement. In order to characterize a given arrangement, two parallel planes are taken, each contains one of the molecular centres and perpendicular to the line connecting them. Then, the classification is performed by the number of corner (or ligand) atoms of each molecule are between the two planes. This way, six different kinds of ideal arrangements have been defined, covering all possible orientations, as corner to corner(1:1), corner to edge(1:2), corner to face(1:3), edge to edge(2:2), edge to face(2:3) and face to face(3:3). Thus, the probability of each arrangement can be determined for any centre-centre distances. The method has contributed to the elucidation of the structure of liquids consisting of regular²⁻⁶ and distorted tetrahedral shapes of molecules^{7,8} and recently, of ionic conductors⁹.

Sulfur hexafluoride (SF₆) is regularly used as an insulator in high-voltage circuit breakers¹⁰. Apart from the technical importance, the high symmetry of the molecules and a peculiar body-centered plastic crystalline phase attracted much attention from a scientific point of view¹¹⁻¹⁶. This phase is stable between the point of sublimation at 223K and phase transition to the low-temperature monoclinic phase¹⁷ occurs at 96K under ambient pressure¹². While the centre of mass of the molecule possesses translational symmetry, apparent molecular rotations are only hindered by neighbouring molecules. Neutron diffraction^{11,12,17} and molecular dynamics (MD) modelling^{14,15} studies that have focused on (among other properties) the orientational ordering of neighbouring molecules usually discussed correlations relative to the ordered crystalline lattice and concluded that fluorine atoms oriented close to the cubic cell axis. While the orientation of the molecule relative to the lattice is frequently taken into account in MD studies addressing the low-temperature phase¹⁸ and the ordered-plastic phase transitions^{19,20}, there are only a few MD^{14,15}, and one¹⁶ Reverse Monte Carlo (RMC) studies that consider local atomic arrangements in terms of atomic RDF-s. The last technique developed originally for liquids and amorphous materials²¹ and provide sets of an atomic configurations consistent with the measured diffraction data without the need to use any potential.

The gaseous, liquid, and supercritical fluid states have triggered only a few diffraction studies^{22,23}. MD simulations are compared to experimental properties on these phases by Dellis and Samios²⁴, using potential sets optimized for describing supercritical fluid²³ and crystalline phases^{13,25}. Strauss et al.²³ used RMC modelling, and their description was focused on atomic RDFs. According to my best knowledge, there has not been any investigation performed yet that would take into

^{a)}Electronic mail: temleitner.laszlo@wigner.hu

account the symmetry of the SF₆ molecule and aim at mutual orientations both in liquid and crystalline phases.

The C₆₀ fullerene has numerous phases depending on temperature and pressure^{26,27}. At low temperature ambient conditions it forms a simple cubic molecular crystal with some disorder. At 260K molecules start to rotate, thus inducing a phase transition²⁸ to the orientationally disordered face-centered cubic structure, stable at and above room temperature. Early diffraction studies^{29–31} clarified the structure of the molecule: they observed a difference between single and double bonds ('D') separating pentagon ('P')-hexagon ('H') and hexagon-hexagon faces, respectively. Concerning the room temperature phase, powder diffraction and RDF (as derived from powder diffraction) studies suggested free and independent rotation²⁸ and a lack of intermolecular ordering³⁰. On the other hand, single-crystal studies provided evidence of slight (within 20% intensity modulation) preferred orientation of molecules³² with more pentagonal than hexagonal faces turning towards nearest neighbour directions³³, and of local ordering of molecules by diffuse scattering^{34–37}.

To describe the structure and take into account orientational ordering, various potential sets have been developed, as reviewed by Launois et. al^{38,39} and Chaplot et. al⁴⁰. These potential sets spread from simple van der Waals interactions on carbons^{41,42}, additional van der Waals centres on double-bonds with charges⁴³, additional charges on single and double-bonds⁴⁴, split charge on double-bonds^{36,45}, anisotropic van der Waals⁴⁶, mean-field⁴⁷ to ab-initio⁴⁸. The main reason to overcome the simple van der Waals potential is that it does not produce the experimentally observed low-temperature phase⁴⁹. Among the reviewed forcefields, none of them is able to describe all of the observed properties³⁹: a mean-field potential set⁴⁷ provided the best match to diffuse scattering. This work found a preference for double-bond to hexagonal or pentagonal faces ('PD' and 'HD') using models of REFS 45 and 47. An examination repeated later⁴⁰ showed the preference of 'HD' and less likely the 'PD' and 'PP' orientations for van der Waals, while the preference of the 'PD' and dislike for the 'PP' orientations by two^{37,44} models. An ab-initio investigation⁴⁸ calculated the interaction energies for dimers and reported the most stable 'HD', 'PP' and 'PD' orientations with 5 meV difference between each other. However, the minimum energy of each orientation is found at different distances, which resulted that for small clusters the 'PP' orientations become preferred, while in crystals the preference of 'PD' is proposed.

In Section II, the orientational correlation formalism of Rey is extended to highly symmetric, nearly spherical shaped pairs of molecules. To demonstrate the applicability of this approach, orientational correlation analysis of condensed phases of the octahedral-shaped sulfur-hexafluoride (SF₆) and room temperature crystalline phase of the truncated icosahedral-shaped C₆₀ are selected. Investigations are based on MD simulations with different forcefields, whose details are presented in Section III. In Section IV the simulations are validated against the measured total scattering powder structure factors for both compounds and additionally, against the density of SF₆. This section contains the analysis of orientational

correlations by the extended method: changes of the studied states for SF₆ by the best performing forcefield, comparison of high-density fluid SF₆ with orientational order in CCl₄ and local order of C₆₀ by different forcefields. Finally Section V summarizes the results.

II. THEORY: GENERALIZATION OF THE ORIENTATIONAL CLASSIFICATION SCHEME

A. Generalization of the classification scheme

To extend the classification scheme introduced by Rey¹ originally for tetrahedral molecules, the question of how many corner atoms of each molecule is between two *planes perpendicular* to the connecting line of molecular centres should be replaced. Instead of *perpendicular planes*, we should consider orientational *cones* with proper *angle* constructed by supposing:

1. The direction of corner atoms from the centre distribute evenly on the surface of a sphere.
2. The average number of corner atoms inside the cone is 2.
3. Only 1, 2, or 3 ligands are allowed to be inside the cone.

The first two conditions determine the half apex angle (γ) of the cone that belong to the molecule possessing N_{corner} corner atoms:

$$\frac{2}{N_{corner}} = \frac{2\pi \int_{\cos\gamma}^1 d(\cos z)}{4\pi} = \frac{1 - \cos\gamma}{2}, \quad (1)$$

after some arrangement:

$$\gamma = \arccos\left(1 - \frac{4}{N_{corner}}\right), \quad (2)$$

is obtained. This corresponds to the definition of a plane in the case of regular or slightly distorted tetrahedral molecules.

On the other hand, the last two conditions for the orientational cone construction states that only one of the P_i probabilities of having i number of corner atoms inside a randomly directed cone exactly determines the other two because this probability for one and three atoms are equal:

$$P_1 = P_3 = \frac{1 - P_2}{2} \quad (3)$$

The derivation and calculation method of P_i from the corner-centre-corner bond angles is presented in Appendix A.

Combining these probabilities for a pair of molecules, the asymptotic values of each group can be obtained for configurations of one kind of molecule having tetrahedral, octahedral and icosahedral symmetries (see TABLE I).

While a specific arrangement of pairs of molecules is categorized unambiguously, the corresponding ideal arrangement

for the group is among the widely used representants (for octahedral molecules figure 1 of REF 14 contains all ideal arrangement except the edge to corner), which facilitate the discussion of the studied system.

Concerning the general case, this method might be used not only for describing mutual orientational correlations between molecules belonging to ‘Platonic’ solids (the un-mentioned cube and dodecahedron are the corner-face duals of octahedron and icosahedron, respectively), but also between their distorted forms, or between their mixtures (like tetrahedral and octahedral), as well. The difference is that the same kinds of classes have different asymptotic probabilities.

B. Correlation function of corner atoms inside the orientation cones

The asymptotic value of a given class of orientation might differ for various high symmetry molecules. However, it is possible to introduce a correlation function that gives an opportunity for directly comparing orientational correlations of *any* high-symmetry molecules, like a tetrahedral to an octahedral one.

According to the conditions supposed previously and considering the connecting line between two molecular centres, the average, the highest and lowest possible numbers of corner atoms within both orientational cones are 4, 6 and 2, respectively. Scaling the highest and lowest numbers of corner atoms to between 1 and -1, a *correlation function of corner atoms inside the orientation cones* is obtained. This function is calculated using the probabilities of orientational correlation classes at a given distance:

$$C_{cic}(r) = p_{3:3}(r) - p_{1:1}(r) + \frac{p_{2:3}(r) - p_{1:2}(r)}{2} \quad (4)$$

III. METHODS

A. Simulations

Classical MD simulations on flexible molecules have been performed by the GROMACS⁵⁰ package using version 2016.3. All simulations used Lennard-Jones interaction parameters and partial charges to model intermolecular and distant intramolecular dispersive and Coulombic interactions. Intramolecular interactions between adjacent atoms are modeled with harmonic bond stretching, angle bending and improper dihedral potentials.

Among the *sulfur-hexafluoride* forcefields reviewed by Dellis and Samios in table 1 of REF. 24, both optimized (referred by the ‘-opt’ postfix) and original forms of Pawley¹³, Kinney²⁵, Strauss²³ and 7Sites (referred as ‘Dellis’) are used here. For calculations at various thermodynamic conditions where measured diffraction datasets are available, both NpT and NVT simulations have been performed in the supercritical state²³ (temperature of 398 K and pressures of 128 bar, 155 bar, 394 bar and 1827 bar), in the orientationally disordered/plastic crystalline^{16,51} phase I (190 K and 1 bar), in

the liquid state close to the triple point (225 K and 10.0552 bar – no measured diffraction data are available here). Only NVT calculations have been performed in the gaseous phase²² (293.15 K and 10.2 bar). Initial configurations containing 5000 molecules are created for gaseous, liquid and fluid phases by randomly placing and orienting molecules into the simulation box determined by the density. In the crystalline bcc phase, each of the 5488 molecules (cell size 14x14x14 of the crystallographic unit cell with 5.89 Å lattice constant) are oriented randomly around equilibrium positions of sulfur.

For carbon tetrachloride, an NVT simulation has been carried out using 10 000 molecules at 300K and a density of 1.59 g/cm³. The parameter set of REF 52 has been used for modeling and molecules were treated as flexible. The bond stretching (205016 kJ/mol/nm²) and angle bending (652.704 kJ/mol/rad²) force constants have been taken from OPLS-AA parameter tables, provided by GROMACS⁵⁰.

Concerning the case of fullerene, three models have been used to model the intermolecular interactions: the ‘Girifalco’⁴¹ forcefield with Lennard-Jones potential on each carbon atom (neutral charges, $\sigma=0.346903$ nm, $\epsilon=0.276427 \frac{\text{kJ}}{\text{mol}}$); the ‘Lu’⁴⁴ forcefield with modified Lennard-Jones parameters on the atoms ($\sigma=0.3407$ nm, $\epsilon=0.28598 \frac{\text{kJ}}{\text{mol}}$) and additional charges on single and double-bonds (0.27e and -0.54e, respectively); and the ‘Sprik’⁴³ forcefield with charges and Lennard-Jones potentials on each carbon atom (0.175e, $\sigma=0.34$ nm, $\epsilon=0.1247 \frac{\text{kJ}}{\text{mol}}$) and on double-bonds (-0.35e, $\sigma=0.36$ nm, $\epsilon=0.1247 \frac{\text{kJ}}{\text{mol}}$), with Lorentz-Berthelot combination rules. In the last case, molecules were kept rigid, while in the first two forcefields the flexible potential set of Monticelli et al.⁴² has been used (bondlengths of 0.14 and 0.145 nm with $392459.2 \frac{\text{kJ}}{\text{mol} \cdot \text{nm}^2}$, bond angles of 120 and 108 degrees with $527.184 \frac{\text{kJ}}{\text{mol} \cdot \text{rad}^2}$, improper dihedrals of 143 degrees with $100 \frac{\text{kJ}}{\text{mol} \cdot \text{rad}^2}$ force constant). For this material, only its plastic crystalline phase is modeled here at room temperature by NVT simulations, starting from an 8x8x8 fcc unit cell (corresponds to 2048 molecules, with lattice constant of 14.16 Å) points as centres of gravity of C₆₀.

During the simulations, the Verlet cut-off scheme has been used with van der Waals cut-off at 2.0 nm (1.0 nm for C₆₀). For electrostatics, the particle-mesh Ewald algorithm has been applied, with the same Coulombic cut-off distance when partial charges were non-neutral. The simulation time step was 1 fs. The configuration energies were minimized first, then equilibrated at different levels: for 0.5 ns Berendsen thermostat ($\tau_T = 0.2$ ps, for C₆₀ it was 2 ps) applied at the right temperature first, then Nose-Hoover thermostat for 2 ns. For NpT runs, an additional 200 ps by Berendsen barostat (with $\tau_p = 1.0$) and at least 1 ns by Parinello-Rahman barostat were done. Carrying out equilibration, production runs were started for 10 ns, saving coordinates at each 100 ps.

In the case of simulations with the ‘Lu’ and ‘Sprik’ forcefields of C₆₀, a modeling sequence at 700K, then at 500K and finally at 300K has been conducted, where each modeling started from the final configuration of the previous simulation.

B. Calculation of total scattering datasets

Numerical datasets were available for the gaseous²² and plastic crystalline phase of SF₆ at 190K^{16,51} while for supercritical fluid states²³ and C₆₀ at room temperature³¹ datasets have been digitized from figures of differential cross-sections and intensity, respectively.

For crystalline phases, total structure factors have been calculated using a new implementation of the RMCPOW method⁵³. For SF₆ 11 configurations were summarized, separated by at least 1 ns of NVT runs, while only the final configuration was taken for C₆₀s. Bragg contributions multiplied by the instrumental resolution function, which was "TOF profile function-2" of GSAS⁵⁴ for SF₆ and Gaussian shape for C₆₀. Their parameters are optimized by a trial configuration.

For other phases, the 'rdf' program of GROMACS summarized the partial RDFs of 101 configurations taken at each 100 ps, which were then Fourier-transformed and weighted according to neutron coherent scattering lengths and composition.

Generally, during the comparison of the measured and simulated total structure factors, the former is rescaled and a constant background is subtracted. For crystalline datasets, the measured pattern rescaled and corrected by 2nd order polynomials above 2.5 Å⁻¹, then it has been compared directly over the full measured range.

IV. RESULTS AND DISCUSSION

A. Validation of the forcefield models

To use configurations taken from MD trajectories for further analysis, it is necessary to validate the forcefields against experimental data. As the following analysis is related to the structural properties, the measured total scattering (powder) structure factor and the densities are compared for SF₆, while only the total structure factor is for C₆₀.

The agreements between measured and NVT MD simulated structure factors of SF₆ are compared in TABLE II by reliability factors. Comparing the performance of different forcefields, the worst agreements are found for the 'Strauss' one for each condition, while other forcefields show similar agreement. It is interesting to note that the non-optimized 'Pawley' forcefield shows the best agreement for some states. As a consequence, the 'Dellis', 'Pawley' and 'Strauss' forcefields are selected to represent the corresponding agreement in FIGURES 1 and 2.

In the gaseous phase (FIGURE 1a), each forcefield provides almost perfect agreements with the measured dataset because the intramolecular structure factor dominates the total structure factor. Focusing on more dense states, the 'Strauss' forcefield total structure factors have not reproduced the measured ones, and close to the triple point liquid phase (FIGURE 1f) large oscillations appeared as the simulated system becomes crystalline. An earlier MD investigation²⁴ also showed that this forcefield results in peak shifts of the total radial distribution function in comparison with the experimental one, while

other forcefields show similar behaviours to each other.

Observing the performance of the other forcefields, agreements at supercritical states (FIGURES 1b-e) are excellent. Only slight differences appear at the low-Q part: the total structure factors of 'Pawley' are slightly less intense than those of 'Dellis': in FIGURE 1d intensity starts to rise below 0.5 Å⁻¹. The other differences between simulated and measured total structure factors can be explained by errors of digitalization. For the plastic crystalline state (FIGURE 2), the simulated patterns provide satisfactory agreement with the total structure factor. Three main differences can be identified: the Bragg-peak intensities; diffuse scattering intensity differences between 1.5 and 5 Å⁻¹; and intensity differences beyond 15 Å⁻¹. The first one might result from MD simulations provided a slightly disordered model in comparison with reality as the simulated intensity of Bragg-peaks become smaller as Q increases. The second one might come that in this range the measured 3 bank datasets overlap, making their alignment slightly difficult. The last one might originate from the limits of harmonic approximation of intramolecular bond lengths and angle bending instead of more realistic approximation for far from its equilibrium value. Here, the 'Dellis' model performs better in comparison with 'Pawley'.

The average densities produced by NpT runs are shown in TABLE III for almost every forcefield. It does not contain gaseous phase datasets, because large volume fluctuations prevented performing NpT simulations, while the 'Strauss' forcefield provided a poor agreement to the total structure factors in the NVT ensemble, so the corresponding NpT simulations have not been done. Comparing the experimental with the simulated densities at 6 states, we can conclude that generally, the optimized and the 7 sites 'Dellis' forcefields perform better even for the 190K and 225K states that are below the applied range used for optimization by Dellis and Samios²⁴. The strong negative difference in the density of the 'Pawley' forcefield for states near the triple point refers to shifts towards the gaseous state, while positive differences for 'Kinney' refer to some transition to the crystalline state.

Taking into account the agreement with experimental density and with neutron total scattering diffraction patterns, the 7 sites 'Dellis' (with partial charges) or the 6 sites 'Pawley-opt' forcefields are recommended to use.

For room temperature C₆₀, simulated and measured patterns are compared in FIGURE 3. Although the overall picture shows satisfactory agreements, discrepancies at the high-Q part have a similar source as for SF₆. They might come from the limitation of the harmonic approximation for bond stretching and angle bending for the flexible 'Girifalco' and 'Lu' potentials, and limitations for fixed distances in the rigid 'Sprik' models. Focusing on the performances of different forcefields, the agreement of 'Sprik' and 'Girifalco' ($R_{wp} = 30.3$ and 30.4 %, respectively) are practically identical, while the 'Lu' one provides the worst agreement ($R_{wp} = 33.43$ %) among the three models and behaves more ordered in comparison with the others. In contrast to SF₆, where best performing forcefields are found, here a variety of models and matching with the total scattering powder pattern is emphasized. The reason is twofold: only selected number of models

are examined, and powder diffraction for C_{60} is not sensitive enough^{32,34} to resolve the weak orientational correlations unambiguously, in contrast to single-crystal diffraction. For SF_6 the corner, edge, and face coordination mean correlation with 1, 2 and 3 atoms, respectively, at the shortest distances for one molecule, while for C_{60} the seemingly 5, 2 and 6 atoms for one molecule should provide somewhat comparable contrast. However, thermal motion and distances of pairs make the unequivocal separation difficult by powder for C_{60} , which was successful only at low-temperatures³⁰.

B. Orientational correlations

1. Condensed phases of sulfur hexafluoride

Following the arguments in Section IV A, from now on the results of simulations with the 7-site 'Dellis' forcefield are used. Sulfur and fluorine positions served as the central and corner atoms, respectively. Then categorization of the orientations of each pair of molecules as a function of centre-centre distances is done, taking into account numbers of corner atoms inside the cones centred on the centre-centre connecting line and having half apex angle of 70.53° , according to II.

First of all, the $C_{cic}(r)$ function is calculated for each state of SF_6 in FIGURE 4 to get a general overview.

Focusing on the short-range order behaviour of non-crystalline states, the functions predict similar behaviour below 5.5 \AA , slightly over the first maximum of the centre-centre radial distribution function. This drop of correlations to zero is explained by the atomic radius of the corner atoms and by simple geometric reasons: if close contact corner atoms of pairs of molecules are densely packed, so the number of corner atoms is higher than average within the orientation cones, the corresponding centre-centre distance is shorter. On the other hand, as the centre-centre distance increases, the number of corner atoms within the cones becomes less. At this range, there are only slight differences between intensities belonging to different states. Nevertheless, two groups are formed: the gaseous and triple point liquid states, and the other fluids. It is interesting to note that the former two are almost on the same isobaric line, while the latter share the same isotherm, but at (at least) 12 times higher pressures than the former two.

Looking at the medium-range order behaviour, the gaseous state does not show any significant correlations beyond the first shell. However, very weak correlations appear in the second coordination shell for the two lowest density supercritical states, and stronger ones for the 1.4 g/cm^3 density state. Concerning the densest supercritical and close to triple point liquid states, their $C_{cic}(r)$ functions show correlations up to the third and even, with low intensity, in the 4th coordination shell. Although both states have roughly the same density, they differ from each other in temperature and pressure, making the close to triple point state correlation function more pronounced. Moreover, even their amplitudes are smaller; these further oscillations have in phase with the centre-centre RDF. We might interpret them as the volume of the atoms are

less mutable, which comes from the first shell behaviour and the increasing density enhances correlations between more distant molecules, both in centre-centre and orientational correlations.

Looking at the $C_{cic}(r)$ of the plastic crystalline state, it differs from the previous phases in the first shell and expresses long-range order behaviour.

To provide a more detailed description, the orientation groups are calculated. The short-range order structure (FIGURE 5) of the non-crystalline states follows the general choreography¹, originating from close packing of corner atoms allows shorter centre-centre distances: first, the drop of 3:3, then the maxima of 2:3 and 2:2 are followed at smaller distances than the first maximum of the molecular centre-centre RDF. Roughly around the maximum of that, intensities of the 1:3 arrangement, then further the 1:2 and 1:1 are raised. It is important to note that as the density of the system increases, it affects only to the intensities approximately over $5.5\text{-}6.0 \text{ \AA}$, leaving the maximum positions intact as the immutable volume of corner atoms predetermined this close contact region.

At larger distances (FIGURES 5 and 6), each molecular centre-centre RDF is in phase with probability modulation of groups having more corner atoms inside the orientation cones (2:3 and 3:3), while it is the opposite for groups having fewer corner atoms (1:1 and 1:2) than the average, corresponding the behaviour found for $C_{cic}(r)$. This expresses that orientational and centre of mass correlations have a common origin. The correlations are allowed to follow clearly to the minimum after the second maximum of centre-centre RDF of the two lowest density fluid states, up to the third maximum for 394 bar and up to the minimum over the 4th shell of centre-centre RDF for the highest density states. It is important to note here that the simulated molecules were flexible and atomic coordinates are used without any further alignment during the calculation of orientational correlations, which slightly biased the asymptotic probability value of some groups (largest deviation: about 0.002 for the 2:2 pairs).

Focusing on the plastic crystalline state at 190 K, the molecular centre-centre RDF (FIGURE 7) exhibits strong thermal displacements from the equilibrium positions. Thus, the nearest neighbours to the $\langle 111 \rangle$, and second neighbours to the $\langle 100 \rangle$ directions of the crystal are overlapping in the radial representation. This behaviour was also observed earlier by Dove and Pawley¹⁴. However, orientational correlations reveal some further features: in the $\langle 111 \rangle$ direction the 3:3 and 2:3 orientations dominate, meanwhile, the 1:3 behaves like in the liquid states and correlations of 2:2 are less abundant. It is interesting to note that the probability of the 3:3 arrangements for close contact is high, while the 2:3 is more competitive with 3:3 for the studied liquids and gaseous states. At farther distances, the probabilities of 3:3 and 2:3 drop to the level of random orientations or even less, which shows the rough limit between the first and second neighbours at 5.5 \AA . Nevertheless, the most significant characteristic of neighbours to $\langle 100 \rangle$ directions is the broad maxima of 1:1 and 1:2 arrangements. In the $\langle 110 \rangle$ direction (between 7 and 9 \AA) the 2:2 and 2:3 arrangements have maxima. Combining the arrange-

ments found, like the maxima of 1:1 to $\langle 100 \rangle$, 3:3 or 2:3 to the $\langle 111 \rangle$ directions, 3 fluorines of each molecule should be placed inside the orientational cones around the cubic body diagonals, and only one fluorine inside the cone around the side of the cubic cell. This suggests preferred orientations of fluorine atoms towards the $\langle 100 \rangle$ direction from the sulfur positions, in accord with earlier studies^{12,15,16}.

2. Orientations in the liquid state: CCl_4 versus SF_6

In the liquid state medium-range order orientational correlations are found, but do they show similar behaviour as in carbon tetrachloride among the tetrahedral shaped molecules, which also possesses medium-range ordering¹?

In order to compare orientational order, the $C_{cic}(r)$ orientational correlation function (FIGURE 8) has been calculated for room temperature liquid CCl_4 ($\rho_{mol} = 0.00622 \text{ \AA}^{-3}$) and for the 1.85 g/cm^3 supercritical SF_6 ($\rho_{mol} = 0.00763 \text{ \AA}^{-3}$). The latter has been selected as the densest non-crystalline state evaluated experimentally by both density and total scattering diffraction. It is obvious from FIGURE 8, that both liquids have a medium-range order: modulations of $C_{cic}(r)$'s are followed beyond the 6th neighbour shell. On the other hand, beyond the 3rd neighbour shell each $C_{cic}(r)$ correlates with the centre-centre RDF (insets of (a) and (b) of FIGURE 8). To separate oscillations originating from the volume of atoms of a spherical-shaped molecules with random orientations at a given density over long-range and not from a specific orientational order, the following probe function, having a form of damped oscillation in the volume of spherical shell, is fitted to $C_{cic}(r)$ beyond 14 \AA :

$$f(r) = \frac{I_0}{r^2} \exp\left(-\frac{r}{\lambda R_0}\right) \cos\left(2\pi \frac{r}{R_0} + 2\pi\phi\right) \quad (5)$$

Performing the fit (TABLE IV), the agreement over the fitted range is almost perfect for SF_6 and good for CCl_4 . Subtracting the fitted $f(r)$ from $C_{cic}(r)$, shorter-ranged correlations are present in the first shell, and very weak ones in the second shell for SF_6 . In contrast, shorter ranged correlations are present in the second neighbour shell and remain distinguishable in the third shell for CCl_4 (FIGURE 8), even though the molecular number density is lower than that is for SF_6 . Thus, SF_6 behaves like a spherical object (having inversion symmetry) in terms of medium-range order, while CCl_4 differs more from it.

Another difference is the intensity of $C_{cic}(r)$ at close contact: it is higher for CCl_4 , where the 3:3 orientational group dominates at the shortest centre-centre distance^{1,3}, while the probability of 3:3 and 2:3 groups for the closest molecules are about 35% for SF_6 (FIGURE 5).

3. Room temperature C_{60}

Omitting the case of endohedral fullerenes, the C_{60} molecule does not have an atom in its centre nor its icosahedral directions. Thus, the centre is calculated as the mean

of atomic coordinates and the centre of each pentagon served as virtual corner atom of the icosahedron at calculations of centre-centre RDF and orientations.

The centre of mass motion differs for flexible and rigid models (FIGURE 9). The individual thermal motion of each carbon atom is taken up by intramolecular motion in the flexible models of 'Girifalco' and 'Lu'. This results in quite distinct centre-centre RDF-s, although the latter is slightly broader than the former. In contrast to them, the centres of the rigid model with the 'Sprik' forcefield mapped all thermal motions of individual carbon atoms and resulted in broad, but distinguishable peaks in the centre-centre RDF.

Focusing on the orientational correlations, the number of virtual corner atoms in the coordination cone should be assigned to the orientation of C_{60} molecule. One corner atom (the "corner") in the coordination cone means the molecule is oriented by a pentagonal face ('P'), while two atoms ("edge") means between the centres of pentagons: on the common edge of two hexagonal faces or the 'double-bond' ('D') in other words. Finally, the "face" coordination realizes an orientation through the hexagonal faces ('H') of the molecule.

Before examining the different models in detail, it is obvious from FIGURES 3 and 9 that solely total scattering powder diffraction for this specific case is not sensitive enough to decide between different models, not even to show convergence in terms of orientational correlations. Being aware of this behaviour, here only the short-range ordering of different models is emphasized.

To quantify orientational correlations within the coordination shell, the probabilities of each group have been averaged over the given shell and normalized by the corresponding random orientation in TABLE V. The averaging have been made between limiting distances, where $g_{cc}(r)$ intensity is 1/10 of the maximum intensity point of the corresponding shell.

In the first coordination shell, which corresponds to the closest atoms to $\langle 110 \rangle$ directions in the crystalline system, the 'Girifalco' model shows a strong preference of 'HH', 'HD' and slight preference of 'DD' orientational groups. This suggests that local arrangements try to avoid to turn into any of the pentagonal faces of them and prefers hexagonal face - hexagonal face or double-bonds at closer and double-bond-double-bond orientation at distant centre-centre distances, which gives a hint about the rotation mechanism. Looking at the second coordination shell ($\langle 100 \rangle$ direction), the opposite 'PP' and 'PD' are favoured strongly by increasing centre-centre distances and the 'DD' slightly, but mainly at closer distances. Even though the observed preference of 'HD' and unlikely of 'PP' and 'PD' found in the first shell agree with earlier study⁴⁰, and agreement with the total scattering powder pattern is satisfactory, it contradicts to single-crystal investigation³³ concerning the preference of pentagonal over hexagonal faces for nearest neighbours.

While the pentagonal coordination was disfavored in the first coordination shell by the 'Girifalco' model, the result by the 'Lu' forcefield shows a clear preference of it, agreeing with³³: both 'PH' (mainly closer distances) and 'PD' (mainly higher distances) kinds of correlations are favoured and the 'PP' arrangement at short distance is more probable. The sec-

ond shell shows less varied arrangements: only the 'DD' arrangement is preferred. This result is in accord with earlier investigation⁴⁰ about the first shell of 'PD' liked and 'PP' disliked, but this model has not agreed well with the total scattering powder pattern.

Interestingly, the 'Sprik' forcefield shows somewhat opposite kind of preference than the 'Girifalco', but the deviations from random values are moderate. The pentagon face related correlations are preferred in the first shell in order of decreasing probability as 'PP', 'PD', 'PH', while in the second shell the hexagonal face related 'HH', 'HD' and 'DD' correlations are the preferred ones. This model showed the best agreement with powder pattern among the three forcefields, the 'PP' and 'PD' preference is in agreement with an ab-initio study⁴⁸. However, the model was rigid.

V. CONCLUSIONS

Based on the results the following statements can be made:

- (i) The orientational correlation scheme introduced originally by Rey¹ is extended to be capable of describing correlations between high symmetry molecules. The orientations of pairs of molecules are classified by the number of corner (aka ligand) atoms for each part found within the orientational cones, whose axes correspond to centre-centre connecting line and spreads from the centre to the direction of the other centre. The extension is made by choosing the apex angle of the orientational cone so that the number of corner atoms spans only from 1 to 3, and the average number for random orientation should be 2. Supposing even distribution of atoms, calculation methods for the half apex angle of the cones and asymptotic probabilities of each class are provided.
- (ii) To demonstrate the applicability of this method, classical molecular dynamics simulations have been performed on gaseous, supercritical fluid, liquid and plastic crystalline phases of sulfur hexafluoride, and on the room temperature plastic crystalline phase of C₆₀, using different forcefields. The performance of each forcefield is validated by comparison to total scattering powder structure factor for both compounds, and additionally to the density for SF₆. For SF₆, the examined set allowed to choose the best among potentials, which was the 'Dellis' overall, and the 'optimized Pawley' (if only 6 sites model without partial charges would be requested).
- (iii) By the analysis of orientational correlations of non-crystalline phases of SF₆ close contact orientation and medium-range order regions are identified. While the former remained almost intact with respect to changes of the density, the rising density increased the range of the latter. Moreover, the $C_{cic}(r)$ function behaved in-phase with the molecular centre-centre RDF.

- (iv) The detailed analysis of different orientational groups for SF₆ showed a similar tendency for the first maximum of orientational groups of increasing distance, which come from geometrical reasons. Concerning medium-range order, oscillations can be followed on groups in high-density states even in the 4th coordination shell. In the plastic crystalline state, close contacts of 3:3, 2:3 correlations are found in the <111> directions, while the second neighbour in <100> showed the preference of 1:1 and 1:2 arrangements. This is in agreement with earlier studies, indicating the preferred orientation of fluorine atoms to <100> directions.
- (v) The medium-range order behaviour of non-crystalline SF₆ is compared with that of liquid CCl₄. The observed phenomenon is explained by the effects of more spherical shape, and the presence of an inversion centre of the SF₆ molecule, in contrast to CCl₄.
- (vi) For room temperature crystalline C₆₀, each orientation groups are calculated for the first and second coordination shells and provide the orientation probability quantitatively as the ratio of the observed and random probabilities for three models. In each case, agreement has been found with earlier studies. As total scattering powder diffraction is not capable of distinguishing between different local orientations (as proved here for 'Girifalco' and 'Sprik' models, with opposite local orientation but almost same structure factors), none of the studied forcefields might be taken as winner. Nevertheless, the 'Sprik' forcefield gave the best performance out of the three forcefields.

As a final remark, this method can be applied to describe orientational correlations of not only Platonic solids, but an exact and distorted form of high symmetry molecules, while the three conditions in II fulfilled. Moreover, it might be applied to not only single component, but mixtures of different high symmetry molecules, or fragments (like mixtures of tetrahedra and octahedra).

ACKNOWLEDGMENTS

The author would like to thank the help for László Pusztai for discussion. The author is grateful that this project was supported by the János Bolyai Research Scholarship of the Hungarian Academy of Sciences and the National Research, Development and Innovation Office(NKFIH), under grant no. KH130425.

DATA AVAILABILITY STATEMENT

The data that support the findings of this study are available from the corresponding author upon reasonable request.

Appendix A: Calculating the random P_i probabilities

In order to determine the P_i values for a given molecule, we should consider that each corner atoms are spaced more or less regularly. Thus each P_i probability corresponds to the surface ratio on a unit sphere, where the axis might pass through and there are i number of atoms *inside the cone* (according to EQ. A2 of REF 1). These domains are also constructed in a complementary way by observing the *overlapping regions* of cones having the same apex angle with the axis passing through on each corner atom. In order to facilitate the calculation the corner (p_c : surface ratio of a cone), the edge (p_e : surface ratio of 2 overlapping cones) and the face (p_f : surface ratio of three overlapping cones) surface ratios composed by the sum of each individual ratios ($p_x = \sum p_{xi}$) on the sphere are introduced (see fig 10). Note, that due to overlapping, the sum of each individual ratios might be more than one.

Connecting them to the P_i probabilities and taking into account that P_3 is exactly equal to p_f and the surface of P_3 contributes to the surface of 3 corners and 3 edges, whereas the P_2 to the surface of 2 corners:

$$P_3 = p_f \quad (\text{A1})$$

$$P_2 = p_e - 3P_3 = p_e - 3p_f \quad (\text{A2})$$

$$P_1 = p_c - 2P_2 - 3P_3 = p_c - 2p_e + 3p_f \quad (\text{A3})$$

Using EQ. 3 and the definition of corner surface ratio we get

$$P_1 = P_3 = p_f = p_e - 1 \quad (\text{A4})$$

$$P_2 = 1 - 2p_f = 3 - 2p_e \quad (\text{A5})$$

Thus, either p_f or p_e should be calculated to determine the P_i probabilities. In the following the p_{ei} is calculated as it only takes into account pair of corner atoms, whose associated parameter (the corner-centre-corner bond angle) is more convenient to use in the case of non-regular shaped objects.

Given the axis of two cones both having the same half apex angle (γ) and separated by α_i degrees from each other. We would like to determine the surface ratio of the common area within the two cones on the unit sphere in comparison with the whole surface. Let's choose a Cartesian coordinate system, direct the 'z' axis to the axis of one of the cones, place 'x' axis in the plane determined by the axes of each cone and 'y' perpendicular to them (see FIG. 11). The surface to be calculated posses two planes of symmetry: one is the 'xz' plane at $y=0$ and the other is the bisecting plane inclined by $\alpha_i/2$ degrees to the z-axis ($\tan \alpha_i/2 = x/z$ on the plane). Taking that small surface element on the unit sphere (S_i), which is limited by the two symmetry planes and the intersecting cone, the corresponding probability:

$$p_{ei} = \frac{4S_i}{4\pi} = \frac{S_i}{\pi}. \quad (\text{A6})$$

In order to calculate S_i , we parametrize its surface to spherical coordinates. Applying the Cartesian-spherical conversion form on unit of spheres $(x, y, z) = (\sin \theta \cos \phi,$

$\sin \theta \sin \phi, \cos \theta)$, the limits are:

$$0 \leq \phi \leq \arccos \left\{ \frac{\tan \alpha_i/2}{\tan \theta} \right\}, \quad (\text{A7})$$

$$\alpha_i/2 \leq \theta \leq \gamma \quad (\text{A8})$$

Thus, the individual ratio is obtained by evaluating the surface integral:

$$p_{ei} = \frac{S_i}{\pi} = \frac{\int_{\alpha_i/2}^{\gamma} \int_0^{\arccos \left\{ \frac{\tan \alpha_i/2}{\tan \theta} \right\}} d\phi \sin \theta d\theta}{\pi} = \frac{\arctan \sqrt{\left(\frac{\sin \gamma}{\sin \alpha_i/2} \right)^2 - 1} - \cos \gamma \arccos \left(\frac{\tan \alpha_i/2}{\tan \gamma} \right)}{\pi} \quad (\text{A9})$$

Introducing the $A = \cos \alpha$ and $G = \cos \gamma$ notations, the individual surface ratio of the edge becomes

$$p_{ei} = \frac{1}{\pi} \left\{ \arctan \sqrt{\frac{1+A-2G^2}{1-A}} - G \arccos \left(\sqrt{\frac{1-A}{1+A}} \frac{G}{\sqrt{1-G^2}} \right) \right\} \quad (\text{A10})$$

Evaluating it to tetrahedral ($A = -1/3, G = 0$), octahedral ($A = 0, G = 1/3$) and icosahedral ($A = 1/\sqrt{5}, G = 2/3$) symmetries, we get:

$$\tilde{p}_{eiT} = \frac{1}{\pi} \arctan \frac{1}{\sqrt{2}} \quad (\text{A11})$$

$$\tilde{p}_{eiO} = \frac{1}{\pi} \left\{ \arctan \left(\frac{\sqrt{7}}{3} \right) - \frac{1}{3} \arccos \left(\frac{1}{2\sqrt{2}} \right) \right\} \quad (\text{A12})$$

$$\tilde{p}_{eiI} = \frac{1}{\pi} \left\{ \arctan \sqrt{\frac{7+5\sqrt{5}}{18}} - \frac{2}{3} \arccos \left(\sqrt{\frac{2(3-\sqrt{5})}{5}} \right) \right\} \quad (\text{A13})$$

The individual surface ratios should be summed up in general, or simply multiplied with the corresponding number of edges in regular (aka Platonic solids) case to obtain p_e , then applying EQ. A4 and A5 to get the P_i random orientation probabilities (TABLE VI).

¹R. Rey, J. Chem. Phys. **126**, 164506 (2007).

²R. Rey, The Journal of Chemical Physics **131**, 064502 (2009).

³S. Pothoczki, L. Temleitner, P. J v ri, S. Kohara, and L. Pusztai, The Journal of Chemical Physics **130**, 064503 (2009).

⁴H. Morita, S. Kohara, and T. Usuki, Journal of Molecular Liquids **147**, 182 (2009).

⁵S. Pothoczki and L. Pusztai, Journal of Molecular Liquids **145**, 38 (2009).

⁶S. Pothoczki, L. Temleitner, and L. Pusztai, Chemical Reviews **115**, 13308 (2015).

⁷S. Pothoczki, L. Temleitner, and L. Pusztai, The Journal of Chemical Physics **132**, 164511 (2010).

⁸S. Pothoczki and L. Pusztai, Journal of Molecular Liquids **225**, 160 (2017).

⁹V. Lacivita, N. Artrith, and G. Ceder, Chemistry of Materials **30**, 7077 (2018).

¹⁰A. Nossair, R. Hawley, and N. Clothier, Nature **206**, 389 (1965).

¹¹J. C. Taylor and A. B. Waugh, Journal of Solid State Chemistry **18**, 241 (1976).

¹²G. Dolling, B. M. Powell, and V. F. Sears, Molecular Physics **37**, 1859 (1979).

¹³G. S. Pawley, Molecular Physics **43**, 1321 (1981).

- ¹⁴M. T. Dove and G. S. Pawley, *Journal of Physics C: Solid State Physics* **16**, 5969 (1983).
- ¹⁵M. T. Dove and G. S. Pawley, *Journal of Physics C: Solid State Physics* **17**, 6581 (1984).
- ¹⁶M. T. Dove, M. G. Tucker, and D. A. Keen, *European Journal of Mineralogy* **14**, 331 (2002).
- ¹⁷J. K. Cockcroft and A. N. Fitch, *Zeitschrift für Kristallographie - Crystalline Materials* **184**, 123 (1988).
- ¹⁸G. S. Pawley and M. T. Dove, *Chemical Physics Letters* **99**, 45 (1983).
- ¹⁹G. Torchet, M.-F. de Feraudy, B. Raoult, J. Farges, A. H. Fuchs, and G. S. Pawley, *Journal of Chemical Physics* **92**, 6768 (1990).
- ²⁰A. Boutin, J. Simon, and A. Fuchs, *Molecular Physics* **81**, 1165 (1994).
- ²¹R. L. McGreevy and L. Pusztai, *Molecular Simulation* **1**, 359 (1988).
- ²²J. G. Powles, J. C. Dore, M. B. Deraman, and E. K. Osa, *Molecular Physics* **50**, 1089 (1983).
- ²³G. Strauss, H. Zweier, H. Bertagnolli, T. Bausenwein, K. Tödheide, and P. Chieux, *Journal of Chemical Physics* **101**, 662 (1994).
- ²⁴D. Dellis and J. Samios, *Fluid Phase Equilibria* **291**, 81 (2010).
- ²⁵K. E. Kinney, S. Xu, and L. S. Bartell, *Journal of Physal Chemistry* **100**, 6935 (1996).
- ²⁶R. Moret, *Acta Crystallographica Section A* **61**, 62 (2005).
- ²⁷M. Álvarez Murga and J. Hodeau, *Carbon* **82**, 381 (2015).
- ²⁸W. I. F. David, R. M. Ibberson, T. J. S. Dennis, J. P. Hare, and K. Prassides, *Europhysics Letters (EPL)* **18**, 219 (1992).
- ²⁹F. Li, D. Ramage, J. S. Lannin, and J. Conceicao, *Physical Review B* **44**, 13167 (1991).
- ³⁰A. K. Soper, W. I. F. David, D. S. Sivia, T. J. S. Dennis, J. P. Hare, and K. Prassides, *Journal of Physics: Condensed Matter* **4**, 6087 (1992).
- ³¹F. Leclercq, P. Damay, M. Foukani, P. Chieux, M. C. Bellissent-Funel, A. Rassat, and C. Fabre, *Physical Review B* **48**, 2748 (1993).
- ³²P. C. Chow, X. Jiang, G. Reiter, P. Wochner, S. C. Moss, J. D. Axe, J. C. Hanson, R. K. McMullan, R. L. Meng, and C. W. Chu, *Physical Review Letters* **69**, 2943 (1992).
- ³³P. Schiebel, K. Wulf, W. Prandl, G. Heger, R. Papoular, and W. Paulus, *Acta Crystallographica Section A* **52**, 176 (1996).
- ³⁴R. Moret, S. Ravy, and J.-M. Godard, *J. Phys. I France* **2**, 1699 (1992).
- ³⁵P. Launois, S. Ravy, and R. Moret, *Physical Review B* **52**, 5414 (1995).
- ³⁶L. S. Chaplot and L. Pintschovius, *Fullerene Science and Technology* **3**, 707 (1995).
- ³⁷L. Pintschovius, S. L. Chaplot, G. Roth, M. Haluska, and H. Kuzmany, *Physica Scripta* **T57**, 102 (1995).
- ³⁸P. Launois, S. Ravy, and R. Moret, *Physical Review B* **55**, 2651 (1997).
- ³⁹P. Launois, S. Ravy, and R. Moret, *International Journal of Modern Physics B* **13**, 253 (1999).
- ⁴⁰S. L. Chaplot, P. S. Schiebel, and L. Pintschovius, *Fullerene Science and Technology* **9**, 363 (2001).
- ⁴¹L. A. Girifalco, *Journal of Physal Chemistry* **96**, 858 (1992).
- ⁴²L. Monticelli, *Journal of Chemical Theory and Computation* **8**, 1370 (2012).
- ⁴³M. Sprik, A. Cheng, and M. L. Klein, *The Journal of Physical Chemistry* **96**, 2027 (1992).
- ⁴⁴J. P. Lu, X.-P. Li, and R. M. Martin, *Phys. Rev. Lett.* **68**, 1551 (1992).
- ⁴⁵L. Pintschovius and S. Chaplot, *Zeitschrift für Physik B Condensed Matter* **98**, 527 (1995).
- ⁴⁶Y. Kita, K. Wako, H. Goto, T. Naito, H. Kawai, and I. Okada, *The Journal of Chemical Physics* **125**, 034506 (2006).
- ⁴⁷K. Michel and J. Copley, *Zeitschrift für Physik B Condensed Matter* **103**, 369 (1997).
- ⁴⁸F. Tournus, J.-C. Charlier, and P. Mélinon, *The Journal of Chemical Physics* **122**, 094315 (2005).
- ⁴⁹Y. Quo, N. Karasawa, and W. Goddard, *Nature* **351**, 464 (1991).
- ⁵⁰M. J. Abraham, T. Murtola, R. Schulz, S. Páll, J. C. Smith, B. Hess, and E. Lindahl, *SoftwareX* **1**, 19 (2015).
- ⁵¹M. G. Tucker and H. Playford, *RMCPProfile Tutorial version 6.5.2* (2015).
- ⁵²M. Zuriaga, M. Carignano, and P. Serra, *The Journal of Chemical Physics* **135**, 044504 (2011).
- ⁵³A. Møllergård and R. L. McGreevy, *Acta Crystallogrphy A* **55**, 783 (1999).
- ⁵⁴A. C. Larson and R. B. Von Dreele, *General Structure Analysis System (GSAS)* (2004).
- ⁵⁵M. Funke, R. Kleinrahm, and W. Wagner, *Journal of Chemical Thermodynamics* **34**, 717 (2002).

TABLE I. Asymptotic probabilities of each groups for different symmetry of molecules obtained by taking into account the $p_{1:1} = p_{3:3} = P_1^2$, $p_{1:2} = p_{2:3} = 2P_1P_2$, $p_{2:2} = P_2^2$ and $p_{1:3} = 2P_1^2$ relations. P_1 is the probability to find one corner atom inside the cone, which is determined on the basis of angular separation of the number of corner atoms (N_{corner}) and half apex angle of the cone (γ).

molecule symmetry	N_{corner}	$\cos \gamma$	γ [°]	$P_1 = P_3$	$P_2 = 1 - 2P_1$	$p_{1:1}; p_{3:3}$ [%]	$p_{1:2}; p_{2:3}$ [%]	$p_{2:2}$ [%]	$p_{1:3}$ [%]
tetrahedral	4	0	90	0.17548	0.64904	3.079	22.779	42.125	6.159
octahedral	6	$\frac{1}{3}$	70.53	0.22075	0.55850	4.873	24.658	31.193	9.746
icosahedral	12	$\frac{1}{3}$	48.19	0.25251	0.49498	6.376	24.997	24.501	12.752

TABLE II. R_{wp} [%] of simulated and measured total scattering structure factors of SF₆ for NVT simulations.

Reference	22	23	23	23	23	51
Temperature [K]	293.15	398	398	398	398	190
Pressure [bar]	10.2	128	155	394	1827	1
Density [kg/m ³]	71.306	850	1000	1400	1850	2374
Kinney	3.59	8.09	10.29	9.84	10.25	27.9
Kinney-opt	3.19	9.61	9.78	11.02	11.69	27.8
Pawley	3.01	7.34	11.41	11.07	9.06	29.3
Pawley-opt	3.28	9.11	9.77	11.10	13.03	27.3
Strauss	4.97	34.1	41.6	34.7	38.0	32.7
Strauss-opt	3.14	9.05	9.24	10.52	11.07	27.6
Dellis	3.15	9.19	9.91	10.89	11.67	27.3

TABLE III. Differences of NpT simulated densities from the experimental one in [kg/m³], using different forcefields for SF₆.

Reference	23	23	23	23	16,51	55
Temperature [K]	398	398	398	398	190	225
Pressure [bar]	128	155	394	1827	1	10.1
Density [kg/m ³]	850	1000	1400	1850	2374	1842
Kinney	114	77	55	91	-4	266
Kinney-opt	-8	-36	-16	45	-69	84
Pawley	-112	-117	-12	118	81	-185
Pawley-opt	-17	-42	-20	34	-45	42
Strauss-opt	-8	-34	-9	57	-43	71
Dellis	12	-14	-3	55	-41	58

TABLE IV. Best fitting parameters of $f(r)$ (EQUATION 5) for $C_{cic}(r)$ over 14 Å for room temperature liquid CCl₄ and for 398 K and 1827 bar SF₆

Molecule	I_0	R_0	λ	ϕ
CCl ₄	14.8(11)	5.205(16)	1.714(61)	0.018(10)
SF ₆	15.9(11)	4.611(16)	1.753(58)	-0.159(13)

TABLE V. Averaged probability of orientation groups normalized by the corresponding random orientational probability for the first and second coordination shell of room temperature C_{60} by different forcefield models. The 'D', 'H', 'P' are refer to double-bond, hexagonal face, pentagonal face, respectively.

Model	Shell	Normalized group probability [%]					
		1:1 'PP'	3:3 'HH'	1:2 'PD'	2:3 'HD'	2:2 'DD'	1:3 'PH'
'Girifalco'	1 st	4	191	23	193	120	33
	2 nd	221	17	153	43	116	60
'Lu'	1 st	55	34	142	63	78	189
	2 nd	30	71	102	100	151	47
'Sprik'	1 st	147	72	121	83	87	109
	2 nd	74	113	90	110	109	91

TABLE VI. Numerical values of random orientation probabilities for some high-symmetry molecules.

symmetry	N_{corner}	N_{edges}	$\cos \alpha/\alpha [^\circ]$	$\cos \gamma/\gamma [^\circ]$	P_{ei}	P_e	$P_1 = P_3 = p_f$	P_2
tetrahedral	4	6	$-\frac{1}{3}/109.47$	0/90	0.19591	1.17548	0.17548	0.64904
octahedral	6	12	0/90	$\frac{1}{3}/70.53$	0.10173	1.22075	0.22075	0.55850
icosahedral	12	30	$\frac{1}{\sqrt{5}}/63.43$	$\frac{2}{3}/48.19$	0.04175	1.25251	0.25251	0.49498

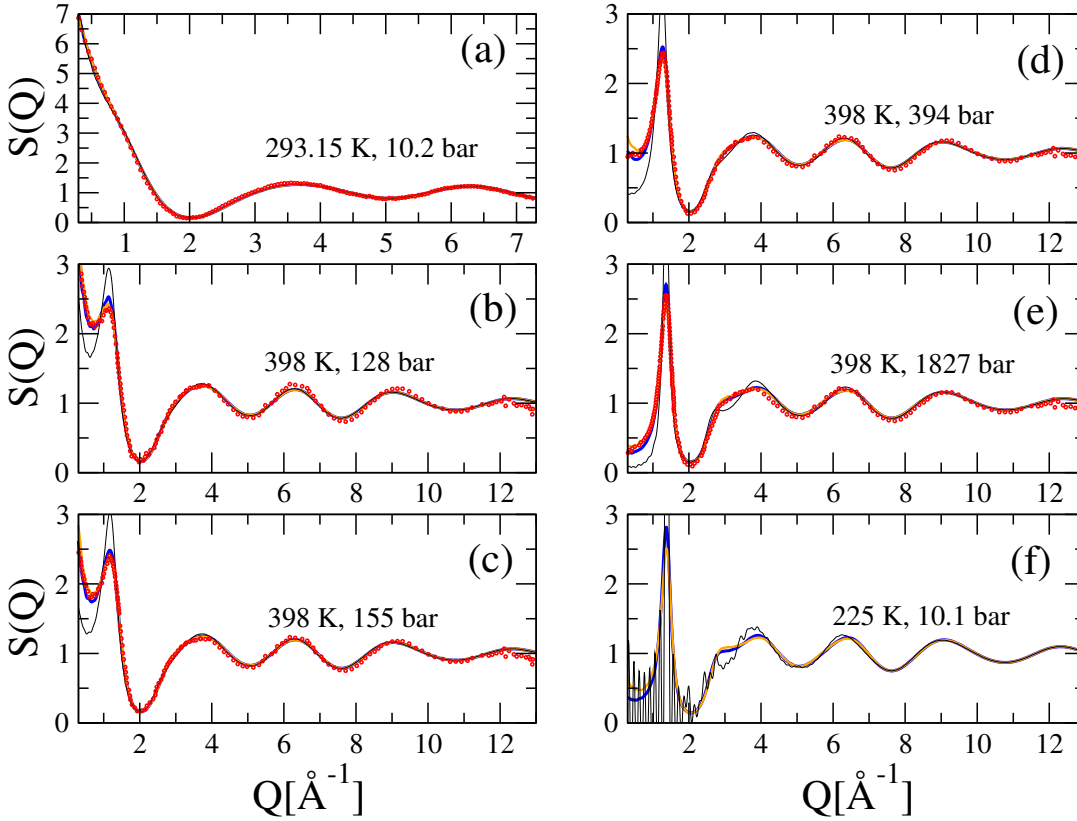


FIG. 1. Comparison of MD simulated and measured total scattering structure factors of gaseous²² (a), supercritical fluid²³ (b)-(e), and prediction for close to triple point liquid state (f) of SF_6 . Measured dataset optimized for 'Dellis' forcefield: red circles; MD with 'Dellis' forcefield²⁴: straight blue lines; with 'Pawley' forcefield¹³: straight orange lines; with 'Strauss' forcefield²³: straight black lines.

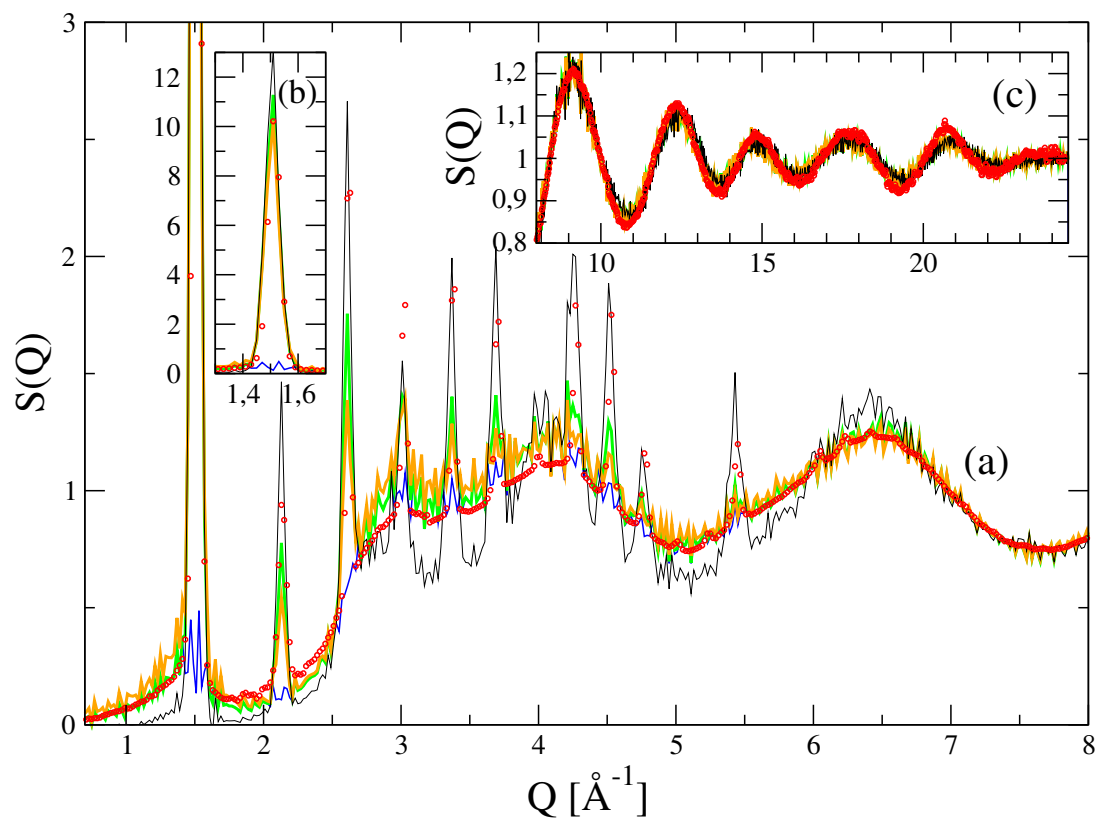


FIG. 2. Comparison of MD simulated and measured⁵¹ total scattering structure factors of SF_6 at 190 K in the plastic crystal state. The low- Q -part is shown on (a), while insets show the agreement at (110) Bragg-reflection (b) and at high Q (c). Measured datasets: red circles; MD with 'Dellis' forcefield²⁴ total (Bragg+diffuse) and only diffuse scattering contributions: straight green and blue lines, respectively; with 'Pawley' forcefield¹³: straight orange lines; with 'Strauss' forcefield²³: straight black lines.

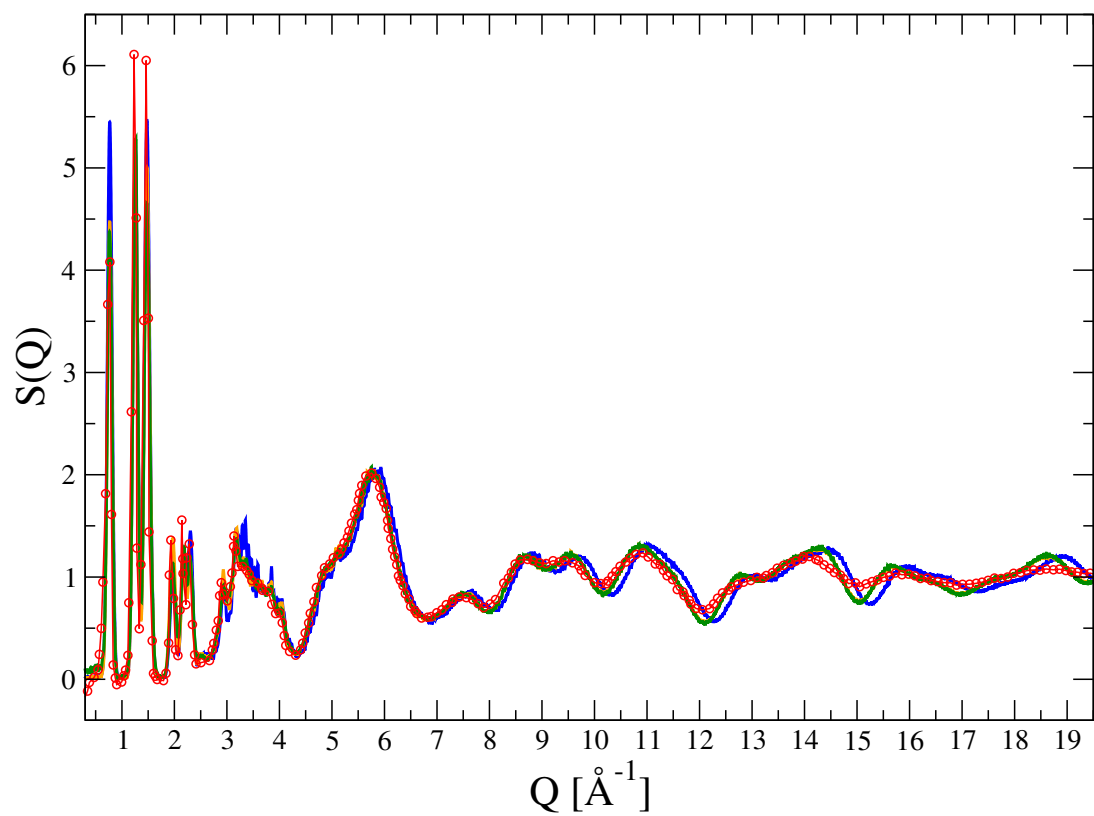


FIG. 3. Comparison of measured³¹ and MD simulated total scattering structure factors of C_{60} at room temperature. Measured dataset: red circles; MD with 'Girifalco' forcefield⁴¹: straight orange line; with 'Lu' forcefield⁴⁴: straight blue line; with 'Sprik' forcefield⁴³: straight green line.

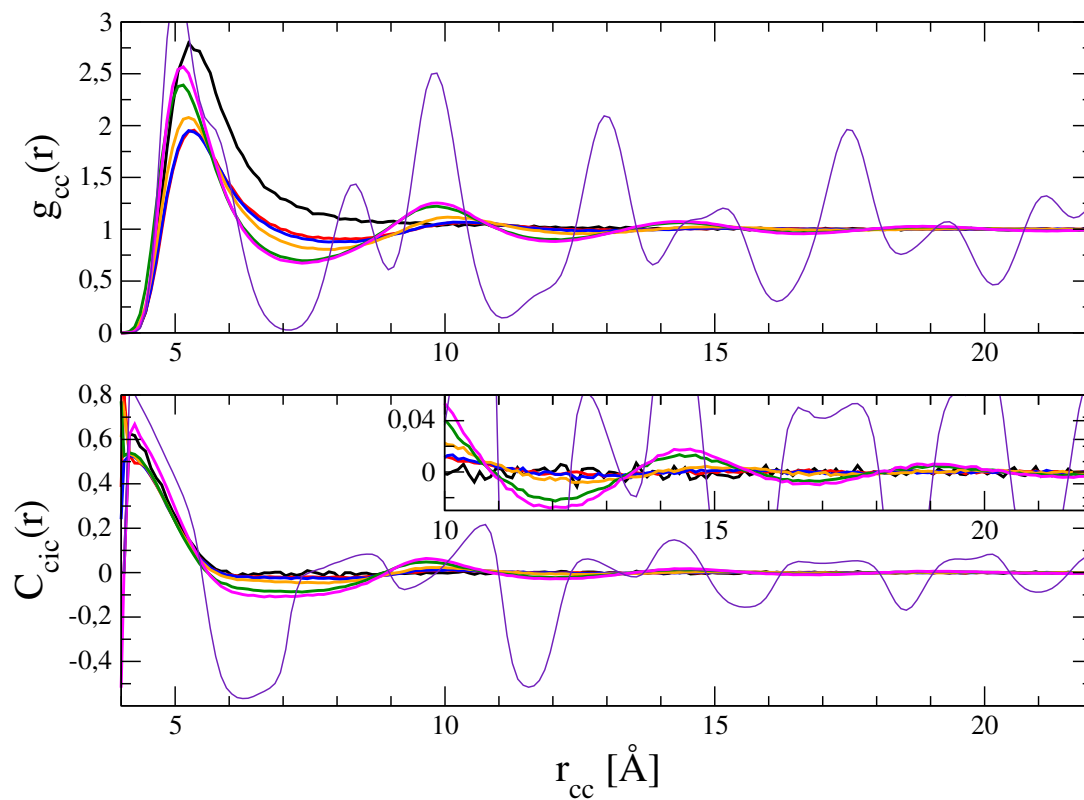


FIG. 4. Molecular centre-centre radial distribution function (upper part) and correlation function of corner atoms within the orientation cones (lower part) in the studied states of SF_6 . The inset shows the least on magnified y scale. 293.15K, 10.2 bar (gaseous): black lines; 398K (supercritical), 128 bar: red lines; 155 bar: blue lines; 394 bar: orange lines; 1827 bar: dark green lines; 225K, 10.1 bar (liquid): magenta lines; 190K, 1 bar (plastic crystal): violet lines.

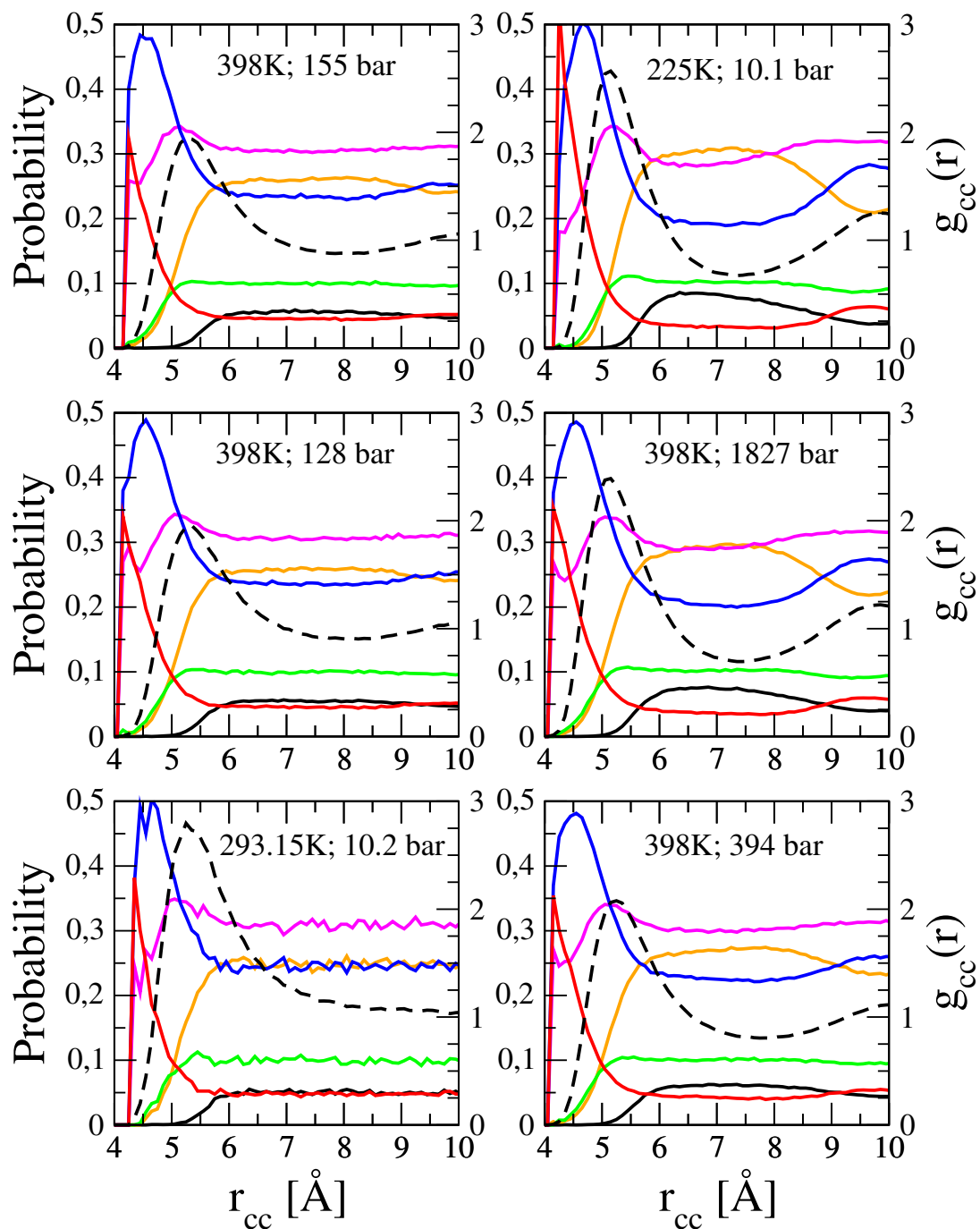


FIG. 5. Orientational correlation probabilities focusing on short-range at 6 non-crystalline states of SF_6 using the classification method of Rey¹. Probability scales are on the left, while scale for the molecular centre-centre radial distribution function (black dashed lines) on the right side of each subfigure. Face-face (3:3): red lines; corner-corner (1:1): straight black lines; edge-face (2:3): blue lines; corner-edge (1:2): orange lines; corner-face (1:3): green lines; edge-edge (2:2): magenta lines.

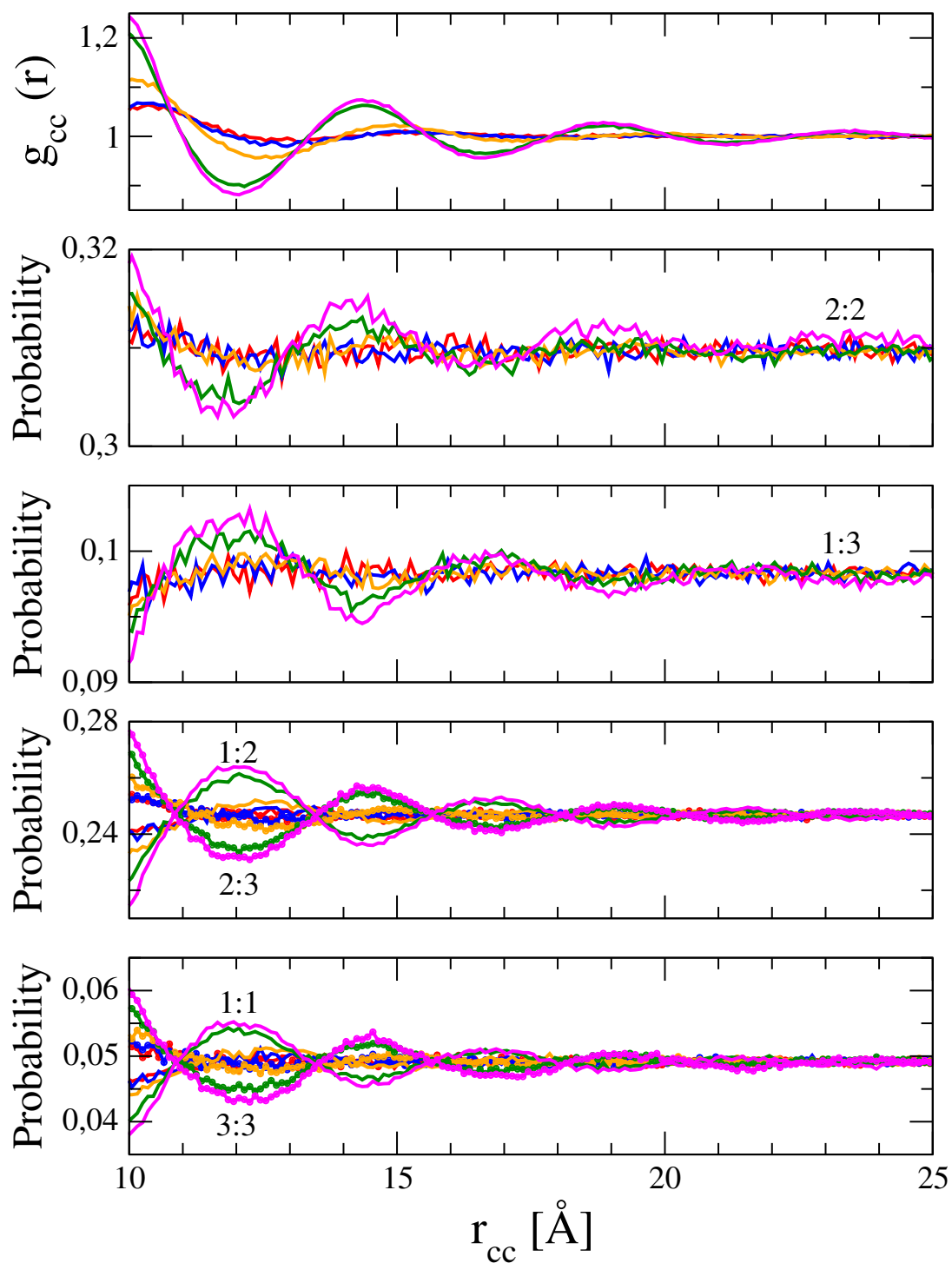


FIG. 6. The molecular centre-centre radial distribution function (on top) and orientational correlation probabilities (the lower 4 subfigures) focusing on the 10 to 25Å range at 5 non-crystalline states of SF₆ using the classification method of Rey¹. 398K (supercritical states), 128 bar: red lines; 155 bar: blue lines; 394 bar: orange lines; 1827 bar: dark green lines; 225K, 10.1 bar (liquid): magenta lines. On the bottom two figures, the groups of 1:1 and 1:2 represented by straight lines, while for 3:3 and 2:3 by straight lines with circles.

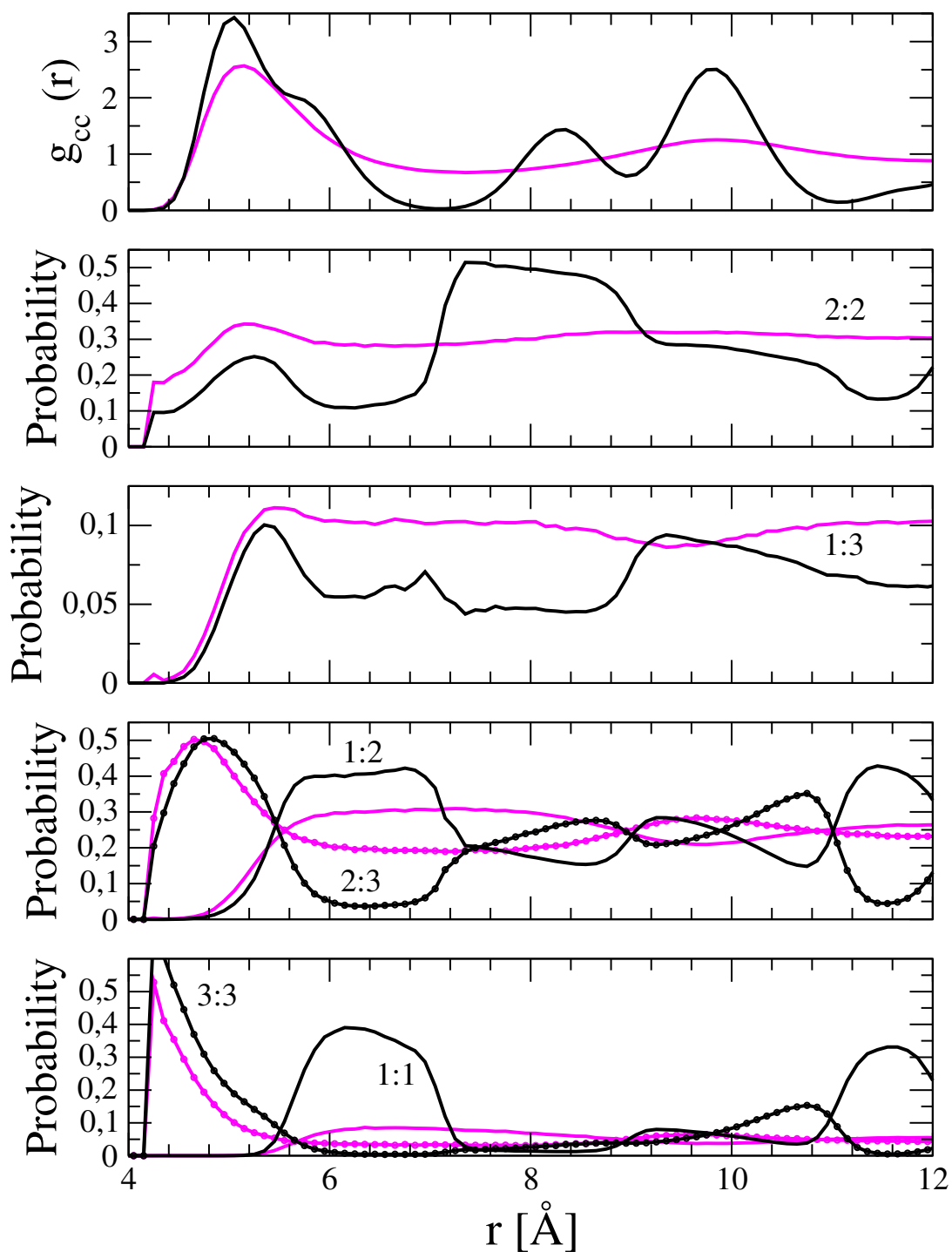


FIG. 7. Comparing orientational correlation probabilities (lower 4 subfigures) in the plastic crystal (190 K, 1 bar, magenta lines) and liquid (225 K, 10.1 bar, black lines) states of SF_6 using the classification method of Rey¹ and the molecule centre-centre radial distribution function (top). On the bottom two figures, the groups of 1:1 and 1:2 represented by straight lines, while for 3:3 and 2:3 by straight lines with circles.

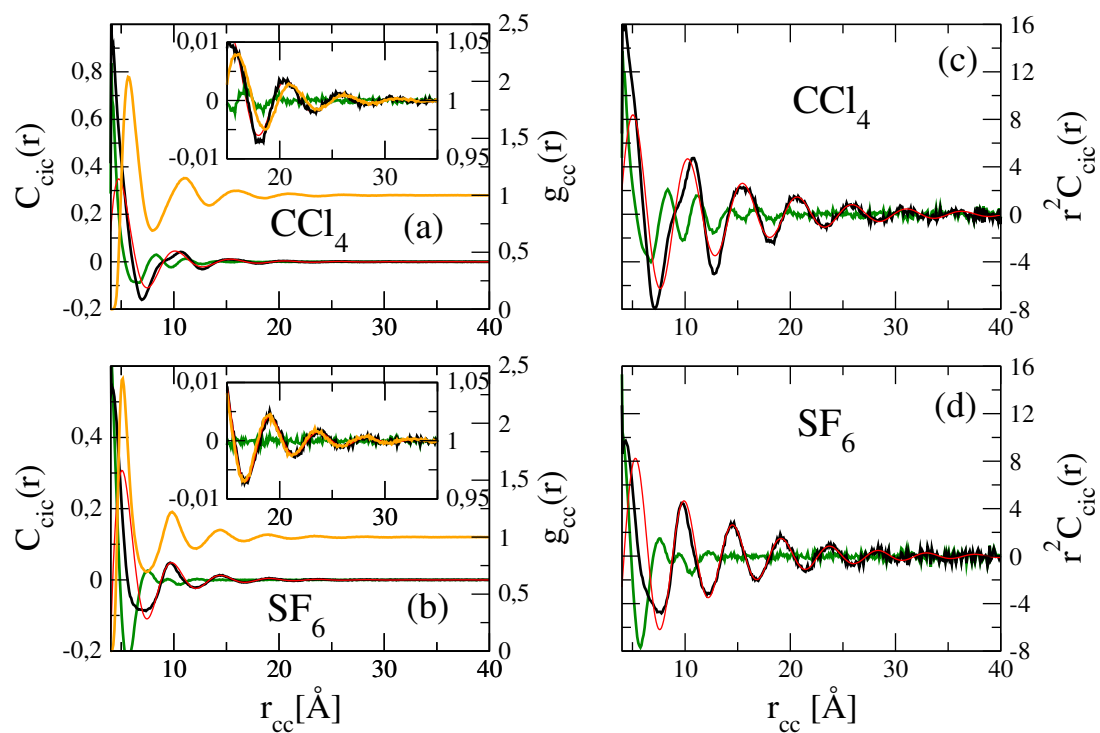


FIG. 8. Comparing the range of orientational correlations in liquid CCl_4 (subfigures (a) and (c)) and in high-density supercritical fluid state (398 K, 1827 bar) of SF_6 (subfigures (b) and (d)) using the $C_{cic}(r)$ (subfigures (a) and (b)) correlation function and its multiplied form (subfigures (c) and (d)). Simulated dataset: straight black lines; fitted $f(r)$ (EQUATION 5): thin red lines; residue: straight green lines; radial distribution function of molecular centres: straight orange lines.

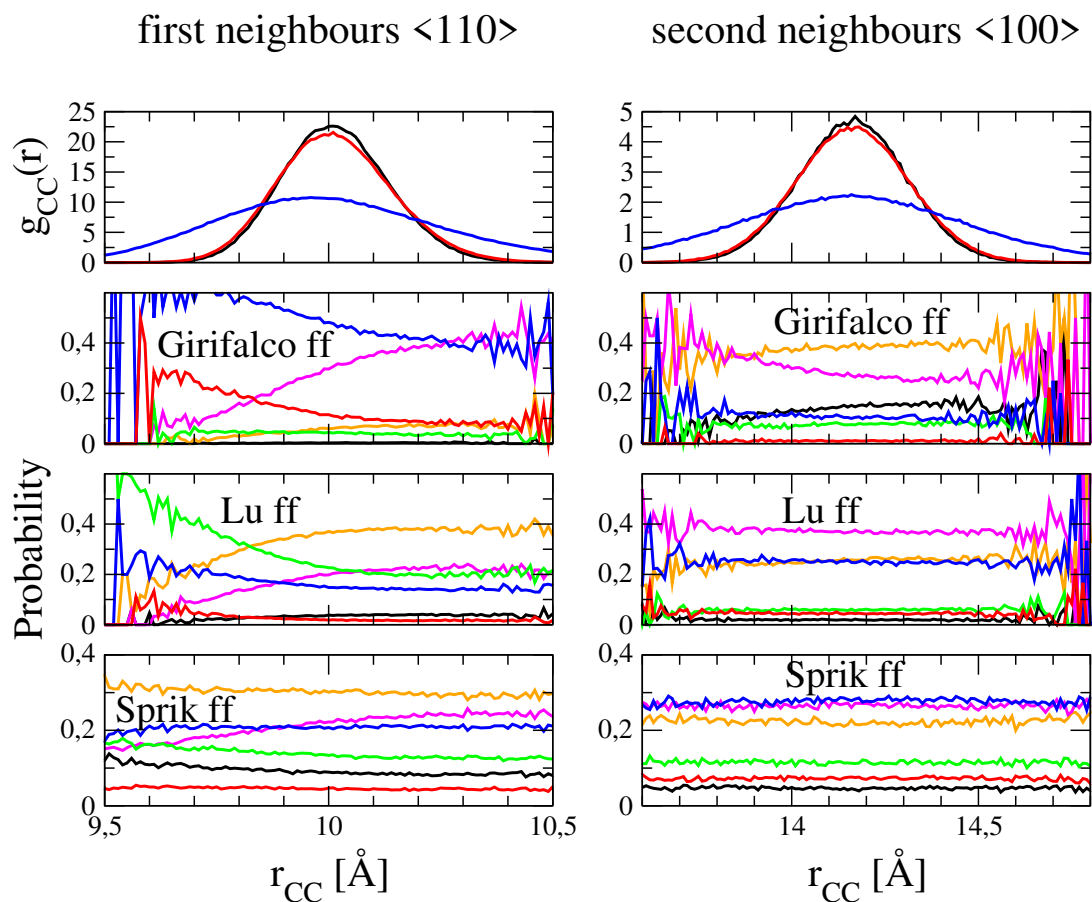


FIG. 9. Molecular centre-centre radial distribution function (uppermost panels) and orientational correlation probabilities (lower panels) using the classification method of Rey¹ for different MD forcefields for the first (left panels) and second (right panels) nearest neighbours of room temperature C_{60} . The examined forcefields are from top to bottom in the lower panels (and color of the lines on the uppermost panels): 'Girifalco'⁴¹ (straight black lines), 'Lu'⁴⁴ (straight red lines) and 'Sprik'⁴³ (straight blue lines), respectively. The colors of different orientational classes on lower panels are arrangements of face-face (3:3, 'HH'): red lines; corner-corner (1:1, 'PP'): straight black lines; edge-face (2:3, 'HD'): blue line; corner-edge (1:2, 'PD'): orange line; corner-face (1:3, 'PH'): green line; edge-edge (2:2, 'DD'): magenta line.

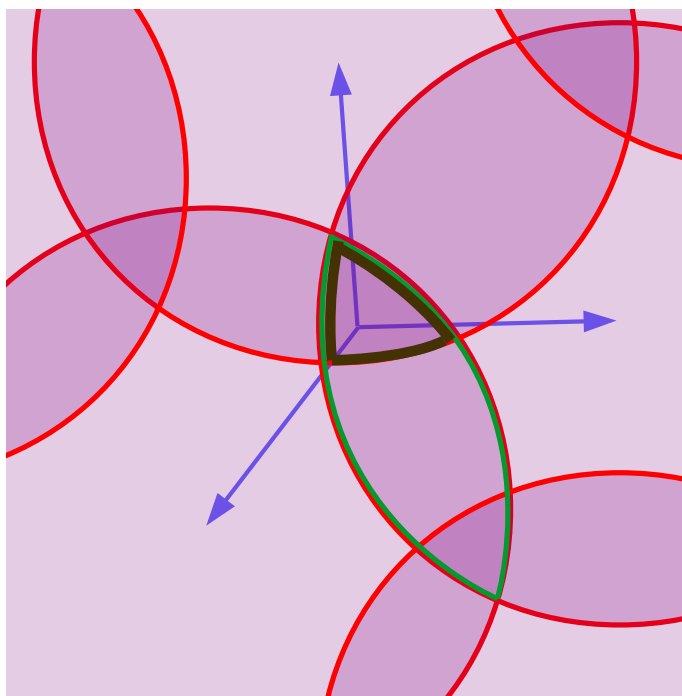


FIG. 10. Surface mapping on the unit sphere. The blue colored arrows point toward ligand atoms from the centre of the molecule serving as axes of cones, which intersects the surface at lines marked by red circles. The light, middle and dark purple regions are surface areas containing 1, 2 and 3 ligands if the molecular centre-centre connecting line pass through them. In order to make calculation of surface ratios easy, individual surfaces of corner, edge and face are defined inside a red circle (p_{ci}), surfaces limited by green (p_{ei}) and brown (p_{fi}) lines are introduced, respectively.

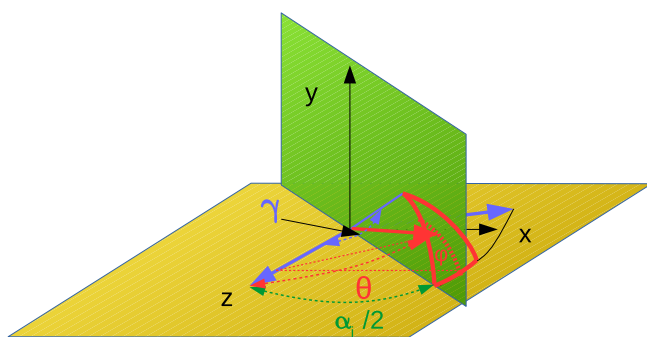


FIG. 11. Calculation of 1/4 of the surface integral belonging to p_{ei} . The surface to be calculated is limited by thick red lines, the blue colored arrows are axis of the cones, whereas planes are represent the symmetry planes.